

Numerical Comparison of the Anastomotic Mechanics of Vascular Grafts Incorporating Blood Flow and Fluid-Structure Interaction

N.K. Schiller^a N.S. Weerasekara^a T. Franz^{b,*} P. Zilla^b
B.D. Reddy^a

^a*Centre for Research in Computational and Applied Mechanics (CERECAM),
University of Cape Town, Private Bag, Rondebosch 7700, South Africa.
Tel.: +27 21 650 3817; Fax: +27 21 685 2281*

^b*Cardiovascular Research Unit, Chris Barnard Department of Cardiothoracic
Surgery, University of Cape, Private Bag X3, Observatory 7935, South Africa.
Tel.: +27 21 406 6418; Fax: +27 21 448 5935*

Abstract

Performance limitations in anastomoses are mainly due to the mismatch in radial distensibility of artery and vascular graft caused by a difference in their mechanical properties, suture material, and suturing techniques. This work aimed at fluid-solid computational investigations of the peri-anastomotic region, with specific reference to the effects of pulsating blood flow. Finite element (FE) and finite volume (FV) models were developed for proximal and distal anastomoses of artery-vein graft and artery-prosthetic graft configurations. FE and FV models were coupled to account for solid-fluid interactions. Emphasis was placed on simplicity of the coupling algorithm. Artery and vein graft showed a larger dilation mismatch in the anastomotic configuration than artery and prosthetic graft. The vein graft distended nearly double compared to the artery - as observed in clinical practice. The prosthetic graft behaved considerably stiffer, displaying approximately half of the arterial dilation. Luminal mismatching was further aggravated by the anastomotic interface itself, forming a pseudo-stenosis in the artery-vein graft anastomosis. While this study focused on end-to-end anastomoses as a vehicle for developing the coupling algorithm, it may serve as useful point of departure for further investigations such as other anastomotic configurations, more refined modelling of sutures, and fully transient behaviour.

Key words: Anastomosis, Vascular graft, Artery, Blood vessel, Blood flow, Computational fluid dynamics, Finite element method,

WORD COUNT: 4950 (excl abstract and bibliography)

1 Introduction

Atherosclerosis, the hardening and narrowing of arteries, is the most common type of arterial disease¹ which is accountable, directly or indirectly, for about half the deaths in the western world. This and other forms of coronary and peripheral vascular diseases are treated by surgical intervention. Bypass grafting uses autologous conduits, such as internal mammary artery and saphenous vein, and prosthetic grafts, typically expanded polytetrafluorethylene (ePTFE) or poly(ethylene terephthalate) (Dacron).² One of the most prominent reasons for poor performance and failure of small and medium sized grafts is the development of anastomotic intimal hyperplasia (AIH), in particular at the distal anastomosis. The causes of AIH range from surgical trauma and lack of endothelium to compliance mismatch and disturbed flow conditions. It is believed that flow conditions and shear stress are the most dominant factors for hyperplastic response.³

The anastomotic configuration and compliance mismatch not only depend on the mechanical properties of host vessel and graft, but also on suture material and suturing technique. Mechanics and compliance mismatch of end-to-side and end-to-end anastomoses have received extensive attention in in-vivo, in-vitro, and numerical studies.^{2,4} Computational approaches have been used to evaluate fluid and structural quantities such as fluid shear stress and circumferential wall stress and strain which are rather difficult to measure in-vivo. The optimization of the anastomotic configuration with regard to fluid and structural mechanics has been a major target of computational studies.⁴

This study investigates, by means of a simple approach, the effects of compliance mismatch between host vessel and vascular graft and suturing techniques on the structural and fluid mechanics of proximal and distal end-to-end anastomoses. The study combines computational solid mechanics, fluid mechanics, and fluid-structure interaction. Anastomotic parameters include three vascular materials (arterial and venous soft tissue, and porous polyurethane) and the interrupted suturing technique. The vascular soft tissue is modelled as a two-layer isotropic, hyperelastic material and the porous polymer as a hyperfoam material. In order to carry out an axisymmetric study, the effect of the sutures is modelled by a smeared-out, orthotropic linear elastic material which is uniformly distributed around the circumference. The blood is assumed to be a Newtonian fluid, with flow being pulsatile and turbulent.

The artery-vein graft anastomoses displayed considerable mismatch of the mechanical behaviour with the diameter increase of the vein graft upon exposure to arterial mean blood pressure being nearly double that of the artery. The

* Corresponding author.

Email address: `thomas.franz@uct.ac.za` (T. Franz).

prosthetic graft behaved far stiffer than the vein graft, here the graft dilation was about 50 % of the arterial dilation. In all cases, the predicted diameter mismatch indicates changes of the physiological flow domain and arterial circulation which is further aggravated by the low-compliant anastomotic interface (suture line). Interestingly, the dilation of the anastomosis, though modeled identically in all cases, showed counterintuitive pattern: a larger dilation was predicted in the stiffer peri-anastomotic configurations of artery-prosthetic graft compared to the more distensible artery-vein graft models.

2 Mathematical Model

2.1 Fluid Dynamics Model

Most generally, blood is modelled as a non-Newtonian fluid. Li et al⁵ mention in their article that “some researchers have shown that when the shear rate reaches 1000 s^{-1} blood behaves as a Newtonian fluid⁶”. But as the shear rate in human arteries can vary between 1 to 1200 s^{-1} over a cardiac cycle,⁷ blood may behave as a non-Newtonian fluid. For simplicity blood is assumed in this study to be an incompressible Newtonian fluid. Conditions are also assumed to be isothermal.

The equations governing the flow of the blood are the equations for conservation of mass and momentum. For incompressible fluids the equation of mass conservation becomes the continuity equation

$$\text{div } \mathbf{v} = 0 \tag{1}$$

where \mathbf{v} is the velocity field.

Neglecting body forces, the equation for conservation of momentum for incompressible Newtonian fluids is given by

$$\rho \frac{\partial \mathbf{v}}{\partial t} + \rho(\mathbf{v} \cdot \nabla)\mathbf{v} = -\nabla p + \mu \nabla^2 \mathbf{v} + \mathbf{V} \tag{2}$$

where ρ is the mass density, μ is the dynamic viscosity, p is the pressure and \mathbf{V} represents terms arising from the additional viscous stress.⁸ Equations (1) and (2) constitute the Navier-Stokes equations.

2.1.1 Turbulence Modelling

Turbulent flows are commonly encountered in practical applications. For most engineering purposes it is unnecessary to resolve the details of the turbulence fluctuations, only the effects of the turbulence on the mean flow are usually required. The time-mean behaviour of these flows is usually of practical interests. Thus, most of the computational procedures solve the time-averaged equations, which supply adequate information about the turbulent process without the need to consider the effects of small scale high frequency fluctuations. Therefore, the equations for unsteady laminar flow are converted into the time-averaged equations for turbulent flow by an averaging operation in which it is assumed that there are rapid and random fluctuations about the mean value. The additional terms arising from this operation are the so-called Reynolds stresses, turbulent heat flux and turbulent diffusion flux.⁸

The low Reynolds number $k - \omega$ turbulence model is used in this work. The type of fluid flow simulated is usually found to be in a transitional region with a Reynolds number around 2000.⁵ Here k is the turbulent kinetic energy and ω is the specific dissipation rate. These variables must satisfy the following two transport equations:

$$\frac{\partial}{\partial t} (\rho k) + \text{div} (\rho k \mathbf{v}) = \text{div} (\Gamma_k \nabla k) + G_k - Y_k + S_k, \quad (3)$$

$$\frac{\partial}{\partial t} (\rho \omega) + \text{div} (\rho \omega \mathbf{v}) = \text{div} (\Gamma_\omega \nabla \omega) + G_\omega - Y_\omega + S_\omega. \quad (4)$$

Here G_k and G_ω represent the generation of turbulence kinetic energy and of ω due to mean velocity gradients. The effective diffusivity is represented by Γ_k and Γ_ω , dissipation due to turbulence is represented by Y_k and Y_ω and lastly the source terms are represented by S_k and S_ω .⁹ These two equations, (3 and 4) need to be solved in order to approximate the stress terms in the governing equations.

To close the system of time averaged conservation equations it is necessary either to relate the extra terms directly to the mean quantities, or to supply additional equations from which they can be derived. A wide variety of turbulent models exists, and it is beyond the scope of this study to review all of these. For further details the reader is referred to the works.^{8,10-13}

2.2 The Anastomosis Model

The solid bodies (the artery and vein grafts as well as sutures) are required to satisfy the equation of motion in the form

$$\rho_s \frac{\partial \mathbf{u}}{\partial t^2} - \operatorname{div} \boldsymbol{\sigma} = \mathbf{0}, \quad (5)$$

in which \mathbf{u} is the displacement, $\boldsymbol{\sigma}$ is the Cauchy stress, and body forces are neglected (see, for example,¹⁴ for a detailed treatment of the material in this section). It is useful also to define the symmetric second Piola-Kirchhoff stress tensor \mathbf{S} ; this is related to the Cauchy stress by

$$\mathbf{S} = J \mathbf{F}^{-1} \boldsymbol{\sigma} \mathbf{F}^{-T} \quad (6)$$

where the deformation gradient \mathbf{F} describes local deformation, and its determinant $J = \det \mathbf{F}$ gives locally the ratio of current to initial volume.

An elastic material is by definition one for which the stress is a function of the deformation only. The assumption of the existence of a strain energy function $U(\mathbf{F})$ together with the principles of material objectivity dictate that the stress is in fact given as a function of $\mathbf{C} = \mathbf{F}^T \mathbf{F}$, the symmetric right Cauchy-Green deformation tensor. Under these conditions we have the general constitutive relation

$$\mathbf{S} = 2 \frac{\partial U(\mathbf{C})}{\partial \mathbf{C}}. \quad (7)$$

It is assumed for simplicity that the arteries and grafts are isotropic, in which case the expression (7) can be specialised further to read

$$\mathbf{S} = \mathbf{S}(I_1, I_2, I_3) \quad (8)$$

in which I_k ($k = 1, 2, 3$) are the three invariants of \mathbf{C} , defined by $I_1(\mathbf{C}) = \operatorname{tr} \mathbf{C}$, $I_2(\mathbf{C}) = \frac{1}{2} [(\operatorname{tr} \mathbf{C})^2 - \operatorname{tr} \mathbf{C}^2]$, $I_3(\mathbf{C}) = \det \mathbf{C}$, and where tr and \det denote respectively the trace and determinant of a tensor or matrix. The stress is now evaluated from

$$\begin{aligned} \mathbf{S} = 2 \frac{\partial U(I_1, I_2, I_3)}{\partial \mathbf{C}} = 2 \left\{ \left(\frac{\partial U}{\partial I_1} + I_1 \frac{\partial U}{\partial I_2} + I_2 \frac{\partial U}{\partial I_3} \right) \mathbb{I} \right. \\ \left. - \left(\frac{\partial U}{\partial I_2} + I_1 \frac{\partial U}{\partial I_3} \right) \mathbf{C} + \frac{\partial U}{\partial I_3} \mathbf{C}^2 \right\}, \end{aligned} \quad (9)$$

where \mathbb{I} is the identity tensor.

2.2.1 Strain Energy Function for Vascular Soft Tissue

In order to model the material properties of the artery as realistically as possible, a strain energy function simulating the hyperelastic properties of the arterial tissue was needed.^{14,15}

The vascular tissue is actually hyperviscoelastic, but as the simulations in this work look at loading conditions within the normal physiological range an approximation of hyperviscoelasticity by hyperelasticity is deemed acceptable.

Delfino et al.¹⁵ have proposed a strain-energy function, which has an isotropic rubber-like strain-energy potential, to model the behaviour of a carotid artery under loading. This strain energy function is used here to define the hyperelastic material properties of arterial and venous soft tissue, and is given by

$$U = \frac{a}{b} \left\{ \exp \left[\frac{b}{2} (I_1 - 3) \right] - 1 \right\} \quad (10)$$

where a is a stress-like material parameter and b is a non-dimensional parameter. With this strain-energy function it was possible to achieve the typical response in the high pressure region.

The assumption is made that the material is incompressible, so that $I_3 = 1$.

The constants used to model the arterial and venous soft tissue sections, mimicing the artery and vein-graft^{15,16} are given in Table 1. A UHYPER adapted from previous work,¹⁵⁻¹⁷ was used to implement these models in *Abaqus*[®].¹⁸

Table 1
Strain Energy Constants for Soft Tissue Layers of Artery (Set 1) and Vein (Set 2)

	Adventitia 1	Media 1	Adventitia 2	Media 2
a	4.74	8.35	2.50	4.71
b (Pa)	27370	44200	20000	27370

2.2.2 Orthotropic Material for Anastomotic Interface

A 2D axisymmetric model was used to simulate the presence of the sutures. The suture properties were incorporated in an averaged sense by replacing the discrete sutures with a continuous band of material with properties which would result in it having the same overall effect of the sutures. As the suture had a much higher stiffness in comparison to the vascular soft tissue and vascular graft sections, this behaviour was modelled by treating the band as

an orthotropic material which was much stiffer in the axial than in the radial directions.

As the deformations in the suture would be small, it was modelled using small-strain elastic theory. In order to simulate the *Prolene*TM suture, based on a previous study¹⁹ a Young's modulus of 18.53 MPa was used. The 12 stitches with two segments each typically found in an anastomosis were approximated to a smear to be modelled in a 2D axisymmetric model. Based on the volumetric composition a volumetric average value of 0.969 MPa for the Young's modulus was computed for a smear in the axial direction and the radial direction value was considered to be 10% of the computed value. The value of Poisson's ratio ν was set at 0.49.

2.2.3 Hyperfoam for Prosthetic Graft Material

The prosthetic graft used is based on porous polyurethane structures produced by methods described by Bezuidenhout et al.²⁰ The graft material which falls into the category of hyperelastic materials was modelled using a hyperfoam model having a strain-energy function described by Yeoman,²¹ Storkers²² and Odgen.²³

$$\begin{aligned}
 U &= U(\bar{\lambda}_1, \bar{\lambda}_2, \bar{\lambda}_3) \\
 &= \sum_{i=1}^n \frac{2\mu_i}{\alpha_i^2} \left[(\bar{\lambda}_1^{\alpha_i} + \bar{\lambda}_2^{\alpha_i} + \bar{\lambda}_3^{\alpha_i} - 3) + 3 \left(J_{el}^{\frac{1}{3}\alpha_i} - 1 \right) + \frac{1}{\beta_i} \left(J_{el}^{-\alpha_i\beta_i} - 1 \right) \right]
 \end{aligned} \tag{11}$$

where λ_i are the principal stretches, $\bar{\lambda}_i = J^{-\frac{1}{3}}\lambda_i$, J_{el} is the elastic volume strain and μ_i , α_i and β_i are temperature dependent material parameters, and are given in Table 2. If all β_i are equal to a constant value β , one can define the effective Poisson's ratio

$$\nu = \frac{\beta}{1 + 2\beta}. \tag{12}$$

These hyperfoam coefficients correspond to the different porogen sizes of the porous structures investigated by Yeoman.²¹

3 Computational Modelling

In order to solve and ultimately simulate the phenomenon being studied in both the solid as well as the fluid problem, the commercial software packages *Abaqus*[®] for the finite element solid modelling, *Gambit*[®] for the mesh

Table 2
Hyperfoam model coefficients²¹

	90 – 106 μm
ν	0.08
μ_1	0.5411×10^6
μ_2	-0.1528×10^6
μ_3	-0.3936×10^6
μ_4	0.1337×10^6
α_1	2.449
α_2	4.694
α_3	-1.575
α_4	-3.571

generation of the flow domain, and *Fluent*[®] to simulate the fluid flow, were used.

3.1 Solid Modelling

The model was subdivided into different partitions, as shown in the section through the walls in Fig. 1. A small partition consisting of two rows of elements at the region of the anastomosis was defined as the suture smear. The remaining divisions of the model, were those of the artery and graft, where an arterial section has been divided again longitudinally to create two equally thick layers representing the media and adventitia. A further partition was created for the graft; in the case of this being arterial in nature, the same procedure as that for the artery section has been followed.

Inner and outer diameters of 4 and 5 *mm* were used respectively for the anastomotic model. Schajer²⁴ suggested a use of length of twice the diameter in modelling anastomosis computationally, thus a 10 *mm* section was chosen for both the artery and the graft, and a 0.2 *mm* for the suture smear was used.

Four-noded bilinear hybrid elements with constant pressure were used in axisymmetric analyses. The mesh generated for this model had to correspond to that used for the fluid domain as the common boundary nodes had to be in the same geometric location. A mesh of 200 elements in the axial direction and 8 elements in the radial direction was chosen. This resulted in 1600 elements defined by 1809 nodes. The inputs loading used for models are given in Table 3.^{15, 25}

Table 3
2D Axisymmetric Model Inputs

INPUT	VALUE
Longitudinal Prestress	10 % of section length
External Pressure	8.6 <i>kPa</i> (65 <i>mmHg</i>)
Luminal Pressure	10.6 – 16.0 <i>kPa</i> (80 – 120 <i>mmHg</i>)

3.2 Fluid Flow Modelling

The flow modelling was carried out using the PISO velocity-pressure coupling algorithm, with the $k - \omega$ turbulence model, discretisation schemes of standard pressure as well as second order upwind for momentum, turbulence kinetic energy and specific dissipation rate were used. A mesh with 40 elements in the radial and 200 elements in the axial direction was created using *Gambit*[®], where a length of 20 *mm* and a radial width of 2 *mm* was considered for the flow domain, with the 200 elements in the axial direction corresponding to the 200 elements of the solid model. A boundary layer consisting of 10 elements from the arterial wall was implemented to create a finer mesh in this region. In addition boundary conditions were assigned to the flow domain. These include a velocity inlet, a pressure outlet, a symmetry axis and a wall boundary.

Peak flow velocities are 0.78 ms in healthy arteries.⁵ The flow velocities used in this work were between 0.25 and 0.5 ms for the preliminary runs. Considerations were made in preliminary modelling where it was assumed that the inlet velocities are fully developed.

In order to model the blood flow through the artery as pulsatile, an initial approximation was made by writing a time dependent user defined function (UDF) using a sinusoidal function to approximate the velocity profile for the duration of one heart beat. Owing to the two phases (diastole and systole) during a heart beat, the function is not truly sinusoidal.

The next step was accomplished by adapting the velocity inflow wave form in Fig. 2.²⁶ Politis *et al*²⁶ base their flow on small arteries with an internal diameter of 4*mm*, and the same dimension was used here. The waveform provided is for 1 second (60 beats per minute), which is an acceptable value for the purposes of this study. It is therefore a realistic physiological pulsatile inflow. A satisfactory representation of the graph was obtained by fitting cubic spline function through the 20 data points. From the spline 1000 data points were obtained, thus giving an input velocity value for every 0.001 s.

3.3 Fluid-Structure Interaction Model

The nature of the problem described is defined by two systems. It is thus essential to study the coupled behaviour of the blood flow and the region of anastomosis. This process can be broken down into the following steps:

- (a) simulation of the blood flow using CFD, and resulting in pressure profile on the arterial wall;
- (b) a finite element analysis of the artery-graft model in which the pressure profile obtained in (a) acts as the loading condition. This simulation gives the displacements corresponding to the solid artery-graft model;
- (c) an updated domain is constructed using the displacements from (b), and the fluid flow simulation is repeated on the new domain;
- (d) the iterative process is repeated until variations in geometry fall below a prescribed tolerance.

The flow and solid domain meshes coincide along the common boundary. This is maintained during deformation of the arteries and grafts. The tolerance specified for the convergence takes the form

$$\frac{d^{i+1} - d^i}{d^i} \leq 1 \times 10^{-4} \quad (13)$$

where d^i is the nodal displacement in the i th iteration of the arterial-graft anastomosis wall. This is checked at every nodal point.

The algorithm is set out in Fig. 3.

A short grid adaptation algorithm refines the nodal values. This is done to ensure that the fine mesh created in pertinent areas, such as at the wall, are not lost, only new nodal values for the common boundary nodes are presented, it is thus necessary to adapt the rest of the grid describing the fluid domain. This is done by keeping axial spacing constant and interpolating radial positions. This has been achieved by setting

$$\frac{y_{2n} - y_{1n}}{y_{bn} - y_{an}} = \frac{y_{2i} - y_{1i}}{y_{bi} - y_{ai}} \quad (14)$$

the subscripts n referring to the new and i to the initial grid values. The subscripts 1 and 2 denote neighbouring nodes, whilst b and a indicate the corresponding boundary and axis nodes respectively.

4 Results and Discussion

Coupled simulations were performed for anastomoses of artery to vein graft and artery to synthetic graft, distinguishing between proximal and distal anastomosis for each case. Results are presented for a operating pressure of 13.3 kPa representing mean arterial blood pressure.

4.1 Artery to Vein Graft

Proximal Anastomosis (Blood Flow from Artery to Vein Graft)

The vein graft dilates more than the arterial region after the longitudinal prestress, external and luminal pressures are applied, see Fig. 5a-c for an operating pressure of 13.3 kPa . This is expected due to the weaker material properties of the vein. The anastomotic interface with the suture behaves less compliantly than both the artery and the vein graft thereby forming a pseudo-stenosis. The inner diameter of the artery and the vein graft increases from 4.0 mm (for both sections at no loading conditions) to 4.5 mm and 4.95 mm , while dilation of the anastomotic interface is limited to 4.06 mm internal diameter. The wall thickness of artery and vein change from 0.5 mm in the unloaded state to 0.42 and 0.38 mm , respectively, at 13.3 kPa pressure. This constitutes a wall thinning of 16.0% and 24.0% in artery and vein.

Figure 4a illustrates the absolute pressure of the fluid domain representing the luminal blood pressure in artery and vein graft. The absolute pressure is obtained as the pressure field, in addition to the operating pressure of 13.3 kPa , once interaction has been established between the deformation of the artery, vein graft and the blood flow. A slight pressure drop is observed at the anastomotic interface. The flow enters a converging region just proximal to the anastomosis, causing an increase in velocity (see Fig. 5a) and a decrease in pressure. As the vein graft dilates distally to the anastomosis, the velocity drops and the pressure rises slightly due to the diffusing effect of the diverging profile. The maximum and minimum pressure lay within the physiological pressure range experienced during a cardiac cycle.

The change in absolute pressure during one cardiac cycle is illustrated in Fig. 4a. The curve for $t = 0.2\text{ s}$ corresponds to the velocity at peak systole (Fig. 2). At this point the blood flow velocity is maximum, the lowest pressure during a cardiac cycle is thus to be expected. The converse is shown for the maximum pressure, which is recorded at the lowest velocities during the cardiac cycle, from $0 - 0.1\text{ s}$ and again between $0.7 - 1.0\text{ s}$. The low velocity at the end of the cardiac cycle allows for a high pressure.

The maximum principal stresses in the media and adventitia are 35 kPa and 10 kPa , respectively, for the artery and 48 kPa and 19 kPa for the vein (see also Fig. 5b). These differences reflect the variation in material properties between media and adventitial layer for each tissue type as well as between the same layer in artery and vein. A stress concentration with a value of 62 kPa is observed at the low-compliance anastomotic interface with the suture line.

Distal Anastomosis (Blood Flow from Vein Graft to Artery)

As in the proximal case, the vein graft is more compliant than the artery, which is confirmed by the results shown in Fig. 5d-f. The pressure drop across the anastomosis is again observed (Fig. 4b), for the same reasons as in the proximal model. It is interesting to note that the absolute pressure is higher throughout the entire anastomotic region for distal case compared to the proximal case (Fig. 4a). This is attributed to the larger distension of the 'inlet' region, formed by the vein graft, in the distal configuration compared to the proximal configuration where the artery represents the 'inlet'.

The distended diameter of the three different vascular regions, namely vein graft, artery, and anastomotic interface, is 4.96 mm , 4.5 mm and 4.06 mm , respectively, which closely matches the values observed in the proximal case. The slight stenosis formed at the anastomotic interface indicates again the effect of the suture. The change in diameter from the larger vein graft to the smaller artery results in an increase in pressure at the centre of the lumen. Due to the sharp dent at the anastomosis, low pressures were recorded along the arterial wall. A similar phenomenon is observed in the velocity profile, where the velocity at the centre of the lumen is high, but decreases quickly with respect to radius.

The wall thinning in both sections agrees with the values observed in the proximal configuration, namely 16.0% in the artery and 24.0% in the vein.

The adventitia and the media layer can be clearly distinguished with respect to maximum principal stress in both vascular sections, see Fig. 5e. The maximum stress is 39 kPa and 30 kPa in the media of vein graft and artery, and 12 kPa and 10 kPa in the adventitia of vein graft and artery.

4.2 Artery to Synthetic Graft

Proximal Anastomosis (Blood Flow from Artery to Synthetic Graft)

In this case, the artery dilates more (internal diameter 4.0 mm to 4.41 mm) than the synthetic graft (4.0 mm to 4.22 mm). The magnitude of the diameter mismatch of the distended artery and synthetic graft is smaller (4.5%) than in the artery to vein graft case (10.0%), resulting in smaller changes of the flow domain (Fig. 6a and c). In addition, the anastomotic interface does not form a stenosis as it distends to 4.24 mm , closely matching the distended graft diameter. The lower diameter mismatch and, more importantly, the absence of an anastomotic stenosis result in a flow domain with nearly constant cross-sectional dimension. This leads to a negligible pressure change across the anastomosis, as opposed to the distinct pressure drop observed in the artery - vein graft case (compare Fig. 4c and a), and the lack of a notable change in the velocity profiles across the anastomotic interface (Fig. 6a).

Differences between arterial and synthetic graft section are also observed in wall thinning. The thickness of the arterial wall, consisting of media and adventitia, is reduced by 18.0% to 0.41 mm which agrees with the value observed in the artery-vein case. A considerably lower wall thinning of 5.0% (wall thickness: 0.5 to 0.48 mm) is however predicted for the synthetic graft.

The media and adventitia of the artery exhibit maximum principal stress values of 38 kPa and 12 kPa , respectively, which are 8.6% and 20.0% higher than those predicted for the proximal artery-vein case. The maximum principal stress in the synthetic graft wall is predicted to 18 kPa . The distribution of the maximum principal stress is illustrated in Fig. 6b.

Distal Anastomosis (Blood Flow from Synthetic Graft to Artery)

The pressurized synthetic graft – artery model (Fig. 6e and f) indicates that, similar to the proximal configuration, the artery dilates slightly more (4.42 mm) than the synthetic graft (4.23 mm) and the anastomotic interface (4.25 mm). The wall thinning in artery and graft is 18.0% and 5.0%, respectively, as predicted for the proximal configuration.

The maximum principal stresses in this configuration are illustrated in Fig. 6e. The media and adventitia of the artery exhibit values of 36 kPa and 11 kPa , respectively, compared to 17 kPa in synthetic graft wall. These values are slightly lower than the respective maximum principal stresses observed in the proximal case. This is attributed to a lower pressure which results, due to energy conservation, from a smaller inlet diameter (synthetic graft: 4.23 mm) compared to the proximal case (artery: 4.42 mm) in combination

with the same inlet velocity. The flow does not show discontinuities across the anastomotic interface, Fig. 6d, and remains similar to the proximal case (Fig. 6a).

4.3 Discussion of Results

The algorithm that has been developed and implemented, though simple in structure, is an effective means for exploring anastomotic behaviour in a fully coupled context. In particular, it has permitted a detailed computational exploration of the behaviour of anastomoses for vein- and prosthetic grafts with arteries.

The results presented show a larger dissimilarity of maximum principal stresses and wall thinning between proximal and distal anastomoses for the artery-vein case compared to the artery-synthetic graft case. This difference can be attributed to the larger discrepancy in mechanical properties between artery and vein leading to a more discontinuous flow domain (Fig. 5a, d) compared to the artery-synthetic graft models (Fig. 6a, d). A notable difference is observed in the distended diameter of the anastomotic interface of 4.06 mm for artery-vein anastomoses and 4.24 and 4.25 mm , respectively, for artery-synthetic graft anastomoses. In combination with larger dilations in the artery-vein model, the anastomotic interface has a stenotic effect, adding to structural and flow discontinuities which finds expression in a considerable anastomotic pressure drop that is not observed for the artery-synthetic graft in absence of an anastomotic stenosis.

The difference in dilation of the anastomotic interface in artery-vein graft and artery-synthetic graft models warrants further investigation. Although the suture and anastomotic technique were modeled identically, the artery-vein interface dilates 1.5% compared to 6.0 and 6.25% , respectively, dilation of the artery-synthetic graft interface. This is in particular surprising since the smaller anastomotic dilation is observed in connection with larger dilation of the graft, i.e. 23.75 and 24.0% for the vein graft compared to 5.50 and 5.75% for the synthetic graft.

Review of the values of wall thinning of all four models indicates an association with the distension of the blood vessel: Increased vessel distension (5.5 , 10.5 , 12.5 , 24.0%) leads generally to increased wall thinning (5.0 , 18.0 , 16.0 , 24.0%). Wall thinning is constituted by (transverse) wall contraction associated with the circumferential wall stretch, and wall compression due to pressure loading. Recalling that all models were analysed at the same operating pressure (13.3 kPa) suggests a dominating role of the wall contraction in the wall thinning process.

The distribution of maximum principal stress in media and adventitia in the arterial sections is fairly similar in all models; maximum adventitial stress levels reach between 29 and 33% of the stress in the media. For the venous sections, the stress in the adventitia reaches similarly 31% of that in the media in the distal configuration whereas it increases to 40% of the medial stress in the proximal anastomosis. The vein in the proximal anastomosis is the section displaying highest stress levels overall, exceeding stresses in venous media and adventitia in the distal anastomosis by 23 and 58%, respectively, although the distended inner vein diameter is nearly the same for proximal (4.95 mm) and distal anastomosis (4.96 mm). The difference in medial and adventitial stresses of vein and artery (the latter serves as reference) are 90 and 37% in the proximal configuration and 30 and 20% in the distal anastomosis. For the synthetic graft, the maximum principal wall stress, in absence of different layers, differ from the stress in arterial media and adventitia by -53 and 50% for the proximal configuration and -53 and 55% for the distal configuration.

Proximal and distal anastomoses were modeled individually by applying the same loading conditions to the inlet boundary which is the artery for the proximal anastomosis and the graft (vein and synthetic, respectively) for the distal anastomosis. The scope of an extended investigation may be to represent the graft as a continuous model extending from proximal to distal anastomosis or to apply the geometric and flow conditions of the outlet of the proximal anastomosis as inlet conditions for the distal anastomosis.

5 Conclusion

The objective of this work was to study the mechanical behaviour of perianastomotic vascular regions using computational techniques, with a particular goals being that of developing and implementing a simple algorithm to account for fluid-structure interaction. The algorithm makes full use of specialised solid and fluid mechanics-based commercial packages, and its key feature lies in a simple iterative procedure for achieving the coupling.

The anastomotic behaviour was reviewed by examining the effects of the suturing and graft material on mismatch in dilation of the host vessel and the graft. In addition, blood flow models were generated to simulate the flow of blood in arteries and grafts, resulting in a better understanding of the properties of this flow phenomenon.

The artery-vein graft anastomoses showed a definitive dilation mismatch, where the vein graft distended to a greater extent than the artery as observed in clinical practice. Here, constrictive external reinforcement of the vein graft will be beneficial to match dilation and flow domains of vein graft and host

artery.^{27,28} While the artery-prosthetic graft peri-anastomotic region showed a lower mismatch in dilation than the artery-vein graft case, the sub-arterial dilation of the prosthetic graft bears problems of different nature, such as longterm patho-physiological changes.²⁹

This study has focused on simple end-to-end anastomoses as a vehicle for developing the algorithm. This initial investigation serves as a useful point of departure for various extensions: for example, other anastomotic configurations, more refined modelling of sutures, and fully transient behaviour. A particular feature that would merit further investigation is that of the counter-intuitive behaviour of the anastomotic interface, with the larger dilation observed in the less compliant artery-prosthetic graft.

Conflict of Interest Statement

The authors confirm that they do not have conflicts of interests in connection with the manuscript submitted and the work and data presented therein.

References

- [1] Noble, A., Johnson, R., Thomas, A., Bass, P., *The Cardiovascular System*, 1st Edition, Elsevier Churchill Livingstone, 2005.
- [2] Tiwari, A., Cheng, K., Salacinski, H., Hamilton, G., Seifalian, A., Improving the patency of vascular bypass grafts: the role of suture materials and surgical techniques on reducing anastomotic compliance mismatch, *Eur J Vasc Endovasc Surg* 25 (2003) 287–295.
- [3] Zilla, P., Bezuidenhout, D., Human, P., Prosthetic vascular grafts: Wrong models, wrong questions and no healing, *Biomaterials* 28 (2007) 5009–27.
- [4] Migliavacca, F., Dubini, G., Computational modeling of vascular anastomoses, *Biomechan Model Mechanobiol* 3 (2005) 235–250.
- [5] Li, M., Beech-Brandt, J., John, L., Hoskins, P., Easson, W., Numerical analysis of pulsatile blood flow and vessel wall mechanics in different degrees of stenoses, *Journal for Biomechanics* 40 (2007) 3715–3724.
- [6] Nichols, W., O'Rourke, M., *McDonald's Blood Flow in Arteries Theoretical, experimental and clinical principles*, 4th Edition, Arnold, London, 1998.
- [7] O'Callaghan, S., Walsch, M., McGloughlin, T, Numerical modelling of newtonian and non-newtonian representation of blood in distal end-to-side vascular bypass graft anastomosis, *Medical Engineering and Physics* 28 (2006) 70–74.

- [8] Patankar, S.V., Numerical heat transfer and fluid flow, Hemisphere Publishing, New York, London, 1980.
- [9] Fluent[®] User Manual (2005).
- [10] Launder, B.E., Spalding, D.B., Mathematical Models of Turbulence, Academic Press, London and New York, 1972.
- [11] Launder, B.E., Spalding, D.B., The numerical computation of turbulent flows, Comp. Meth. Appl. Mech. Eng. 3 (1974) 269–289.
- [12] Peric, M., A finite volume method for the prediction of three-dimensional fluid flow in complex ducts, Ph.D. thesis, University of London (1985).
- [13] Versteeg, H.K., Malalasekera, W., An Introduction to Computational Fluid Dynamics, Pearson Prentice Hall, Harlow, 1995.
- [14] Holzapfel, G., Gasser, T., Ogden, R., A new constitutive framework for arterial wall mechanics and a comparative study of material models, Computational Biomechanics 61 (2000) 1–48.
- [15] Delfino, A., Stergiopoulos, N., Moore, J.E., Meister, J.J., Residual strain effects on the stress field in a thick wall finite element model of the human carotid bifurcation, J. Biomechanics 30 (1997) 777–786.
- [16] Koch, T., Non-linear finite element analyses of the aortic heart valve, Master’s thesis, University of Cape Town (2004).
- [17] Schaefer, M., Numerical investigation of the mechanical behaviour of anastomotic regions in vascular grafts, BSc thesis, University of Cape Town (2006).
- [18] Abaqus[®] User Manual (2004).
- [19] Aguirre, A.F., Oliva, M., Schoepfoerster, R.T., Kasyanov, V.A., Static and dynamic mechanical testing of a polymer with potential use as heart valve material, in: Summer Bioengineering Conference, June 25-29, Key Biscayne, FL, USA, 2003.
- [20] Bezuidenhout, D., Davies, N., Zilla, P., Effect of well defined dodecahedral porosity on inflammation and angiogenesis, ASAIO J 48 (2002) 465–71.
- [21] Yeoman, M., The design and optimisation of fabric reinforced porous prosthetic grafts using finite element methods and genetic algorithms, Ph.D. thesis, University of Cape Town (2004).
- [22] Storkers, B., On material representation and constitutive branching in finite compressible elasticity, Journal of the Mechanics and Physics of Solids 34(2) (1986) 125–145.
- [23] Odgen, R.W., Non-linear elastic deformations., Wiley and Sons, 1984.
- [24] Schajer, G., Green, S., Davis, A., Hsiang, Y., Influence of elastic nonlinearity on arterial anastomotic compliance, Journal for Biomedical Engineering 118 (1996) 445–451.

- [25] Zhang, W., Liu, Y., Kassab, G.S., Flow-induced shear strain in intima of porcine coronary arteries, *Journal of Applied Physiology* 103 (2007) 587–593.
- [26] Politis, A., Stavropoulos, G., Christolisa, M., Panagopoulos, P., Vlachos, N., Markatos, N., Numerical modelling of simulated blood flow in idealized composite arterial coronary grafts: Transient flow, *Journal of Biomechanics* 41 (2008) 25–39.
- [27] van der Merwe, H., Reddy, B.D., Zilla, P., Bezuidenhout, D., Franz, T., A computational study of knitted nitinol meshes for their prospective use as external vein reinforcement, *J Biomech* 41 (2008) 1302–1309.
- [28] Zilla, P., Human, P., Wolf, M., Lichtenberg, W., Rafiee, N., Bezuidenhout, D., Samodien, N., Schmidt, C., Franz, T., Constrictive external nitinol stenting of vein grafts inhibits intimal hyperplasia in non-human primates, *Journal of Thoracic and Cardiovascular Surgery* In press.
- [29] Seifalian, A.M., Giudiceandrea, A., Schmitz-Rixen, T., Hamilton, G., Noncompliance: The silent acceptance of a villain, In: *Tissue Engineering of Vascular Grafts*. Zilla, P., Greisler, H.P. (Eds.), RG Landes Co, Austin, Texas (1999) 47–58.

Figure captions

Fig. 1. 2D axisymmetric partitioning of peri-anastomotic vascular wall.

Fig. 2. Inlet flow velocity profile ($\phi_{internal} = 4mm$).²⁶

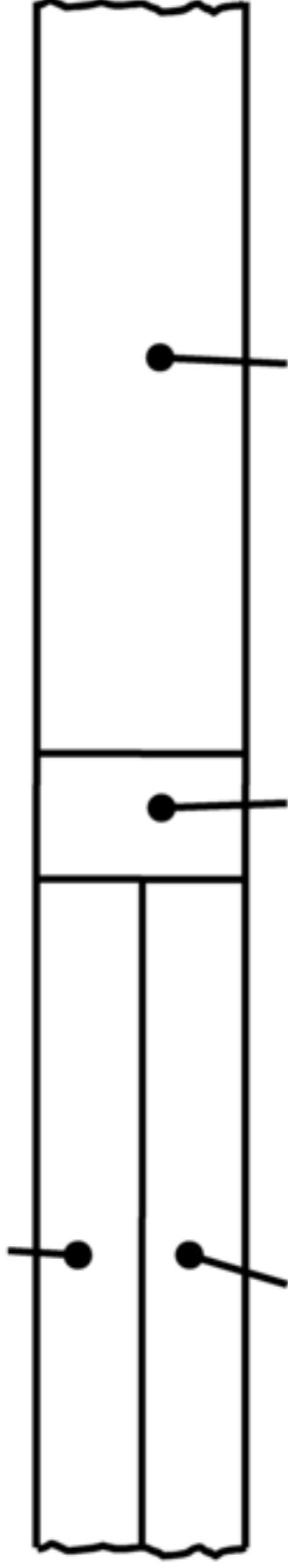
Fig. 3. Sequence of the coupled simulation.

Fig. 4. Plots showing the absolute pressure along the anastomosis wall at different times during the cardiac cycle. (Colour version available as supplementary online material.)

Fig. 5. Predicted blood flow profiles and flow induced stress in artery to vein graft anastomosis. Note: Blood flow from left to right. (Colour version available as supplementary online material.)

Fig. 6. Predicted blood flow profiles and flow induced stress in artery to prosthetic graft anastomosis. Note: Blood flow from left to right. (Colour version available as supplementary online material.)

Adventitia



Media + Intima

Suture

Prosthetic Graft

Figure 2
[Click here to download high resolution image](#)

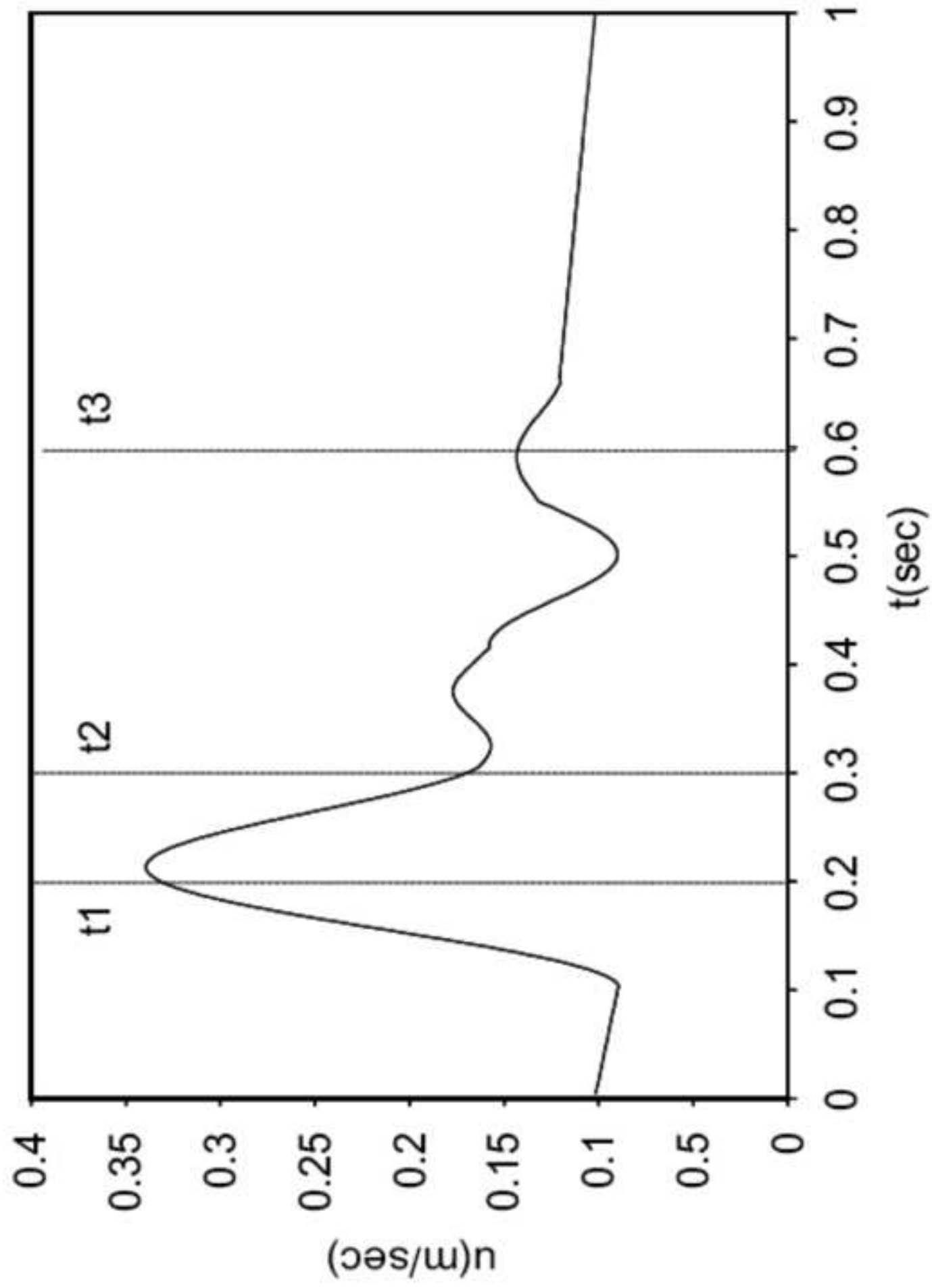


Figure 3
[Click here to download high resolution image](#)

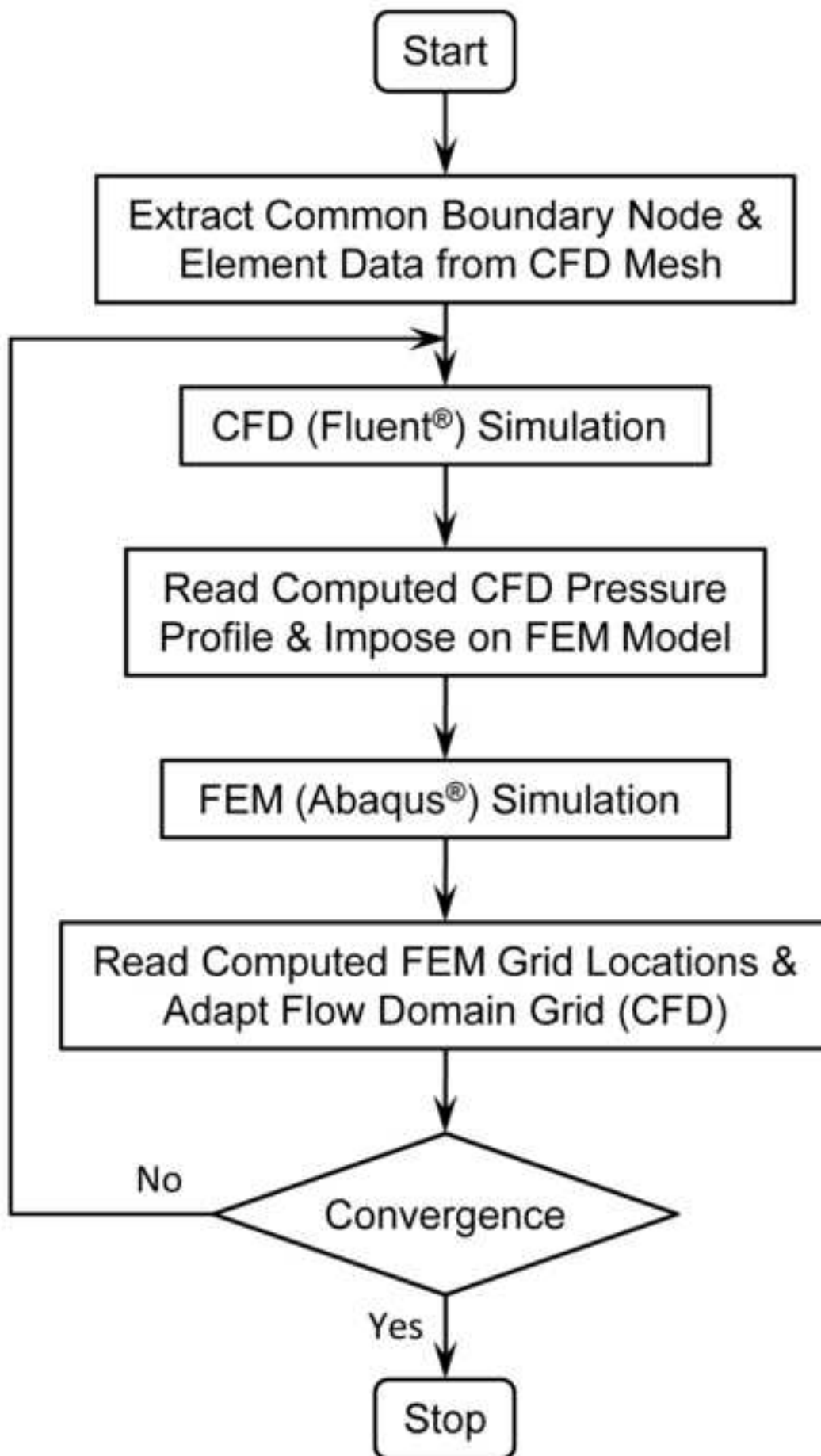
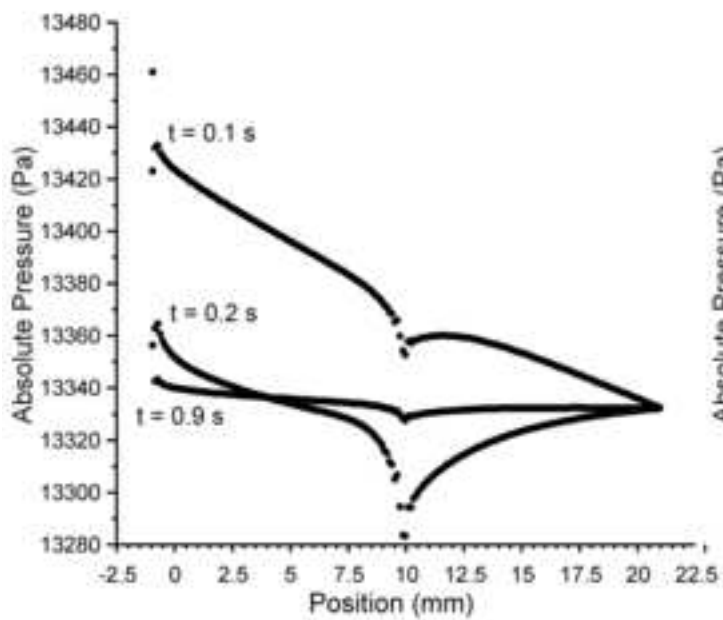
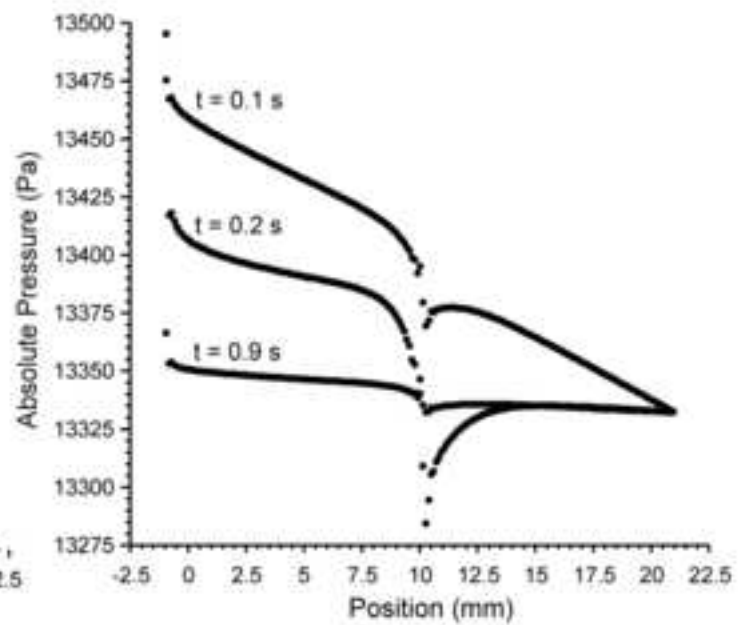


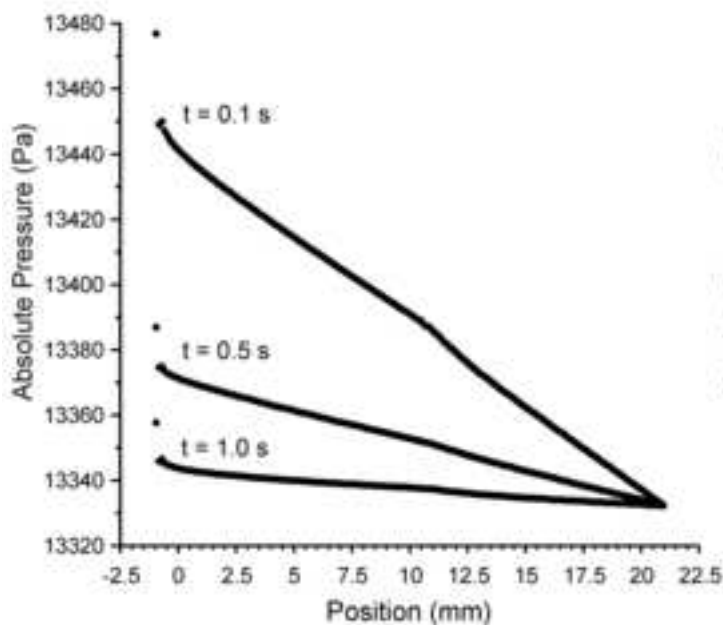
Figure 4
[Click here to download high resolution image](#)



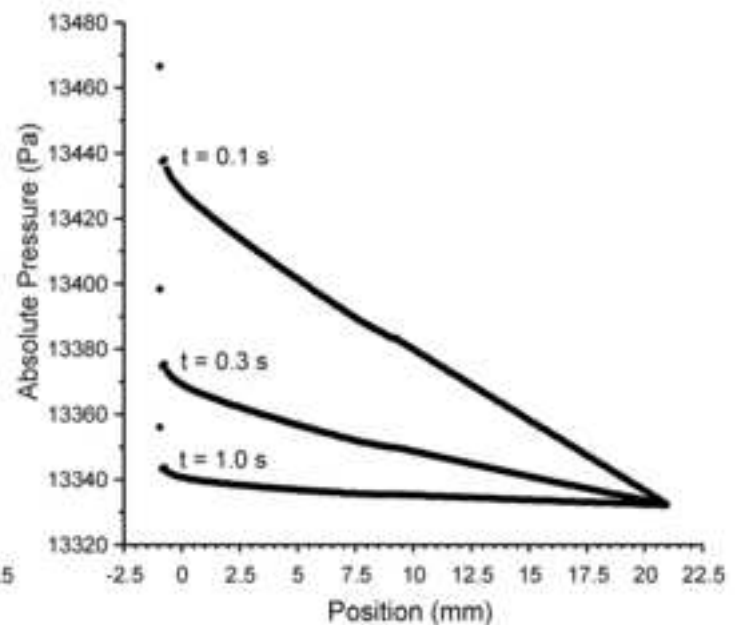
(a) Proximal artery to vein graft model (Artery - Graft)



(b) Distal artery to vein graft model (Graft - Artery)



(c) Proximal artery to prosthetic graft model



(d) Distal artery to prosthetic graft model

Figure 5

[Click here to download high resolution image](#)

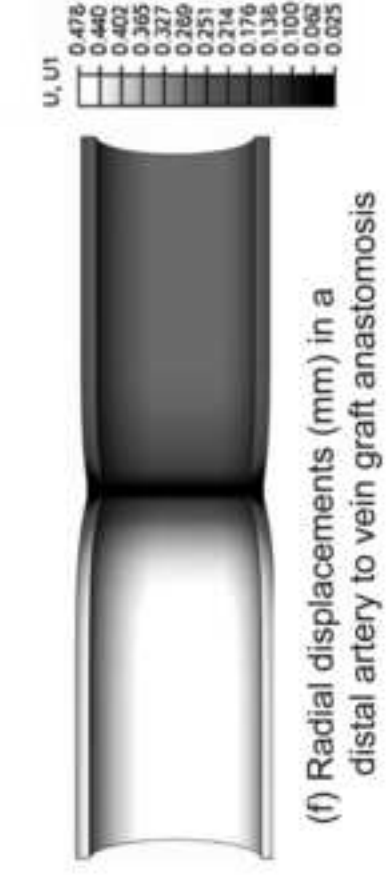
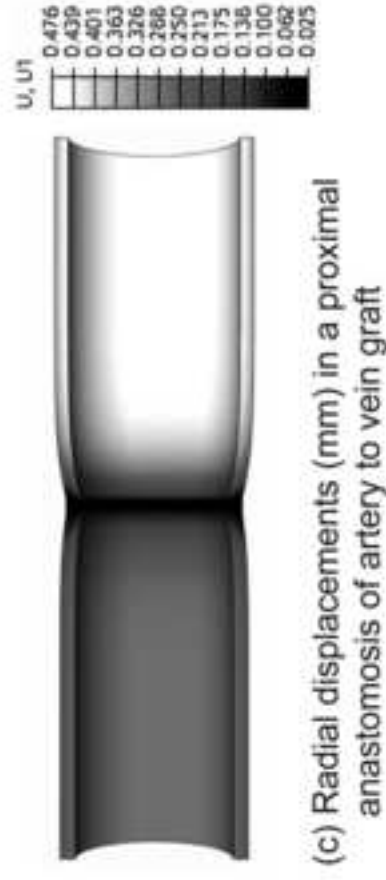
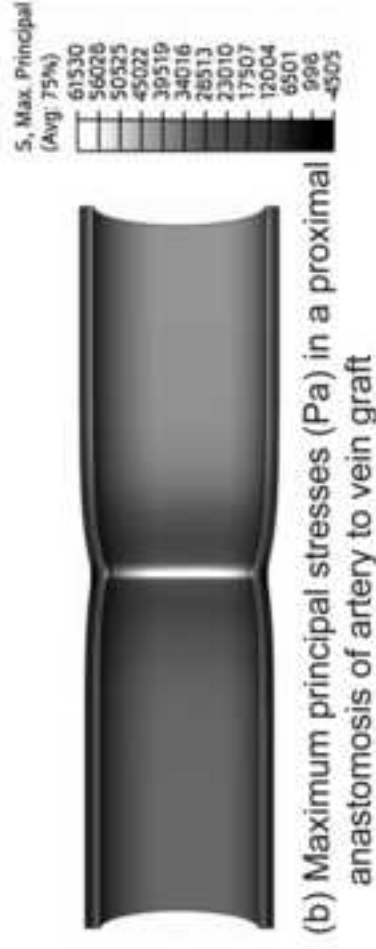
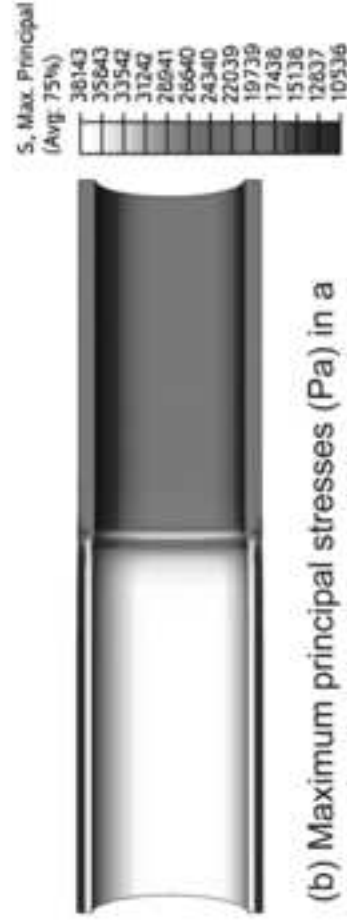
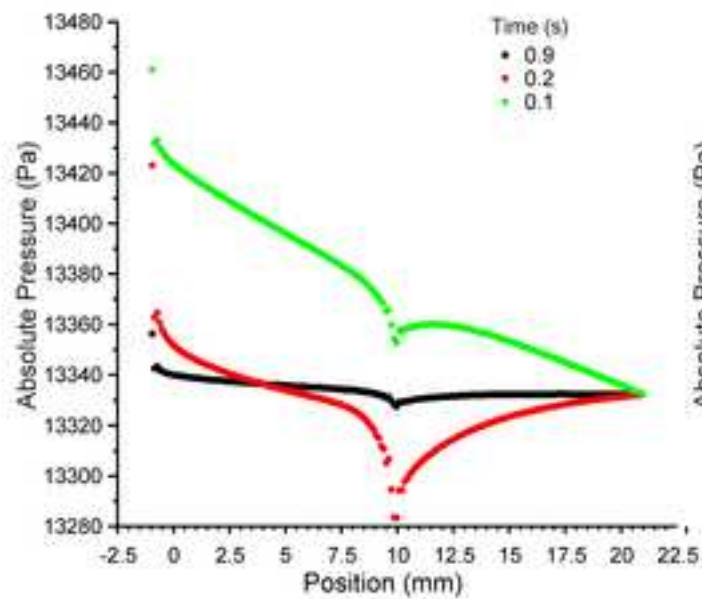


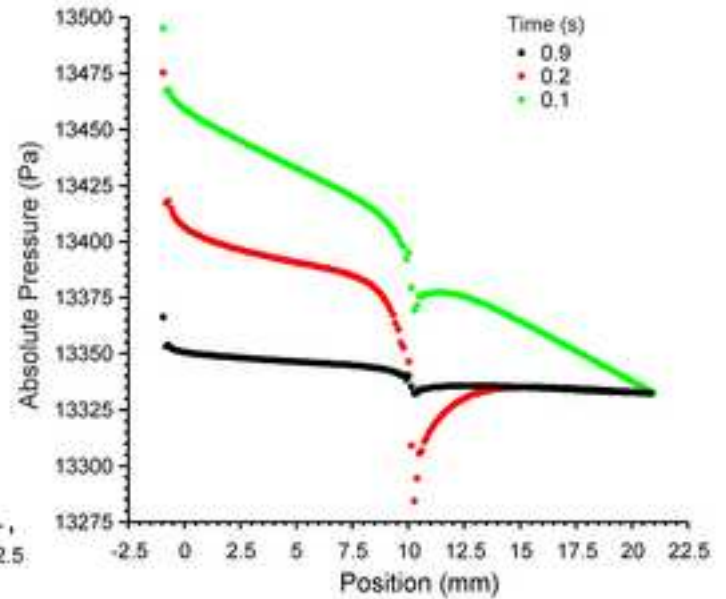
Figure 6

[Click here to download high resolution image](#)

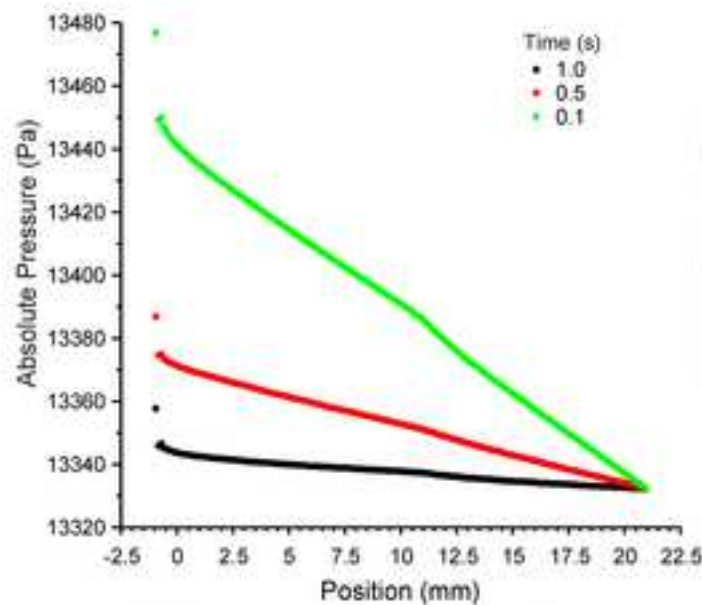




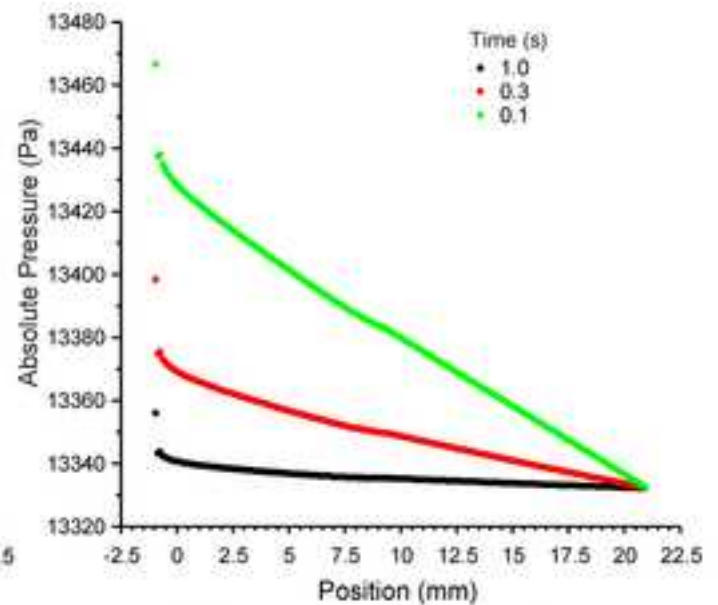
(a) Proximal artery to vein graft model (Artery - Graft)



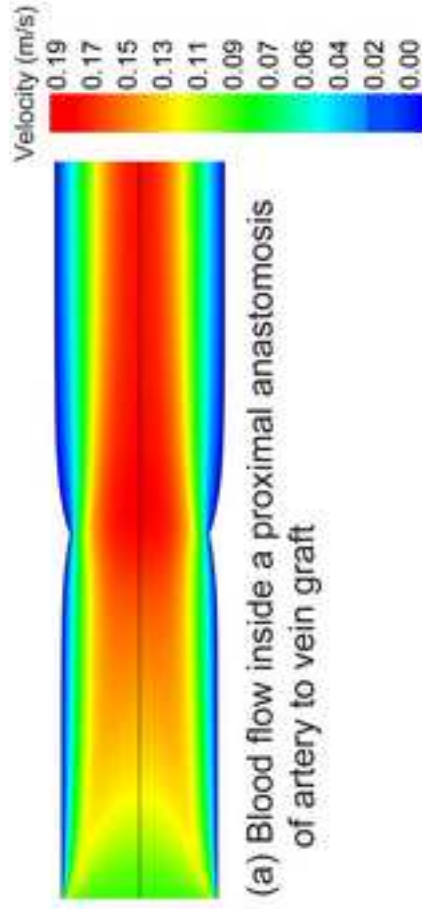
(b) Distal artery to vein graft model (Graft - Artery)



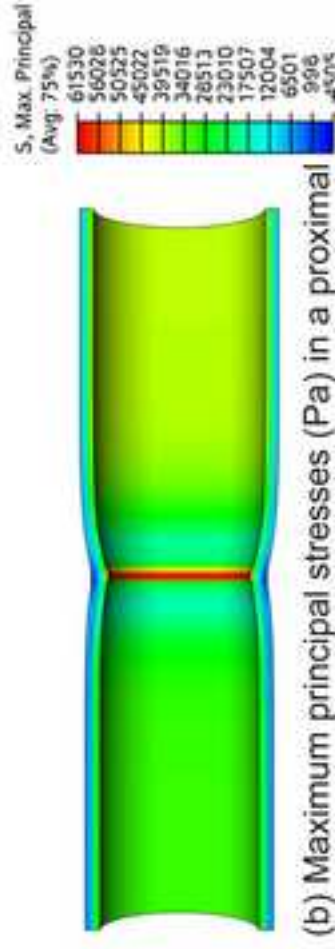
(c) Proximal artery to prosthetic graft model



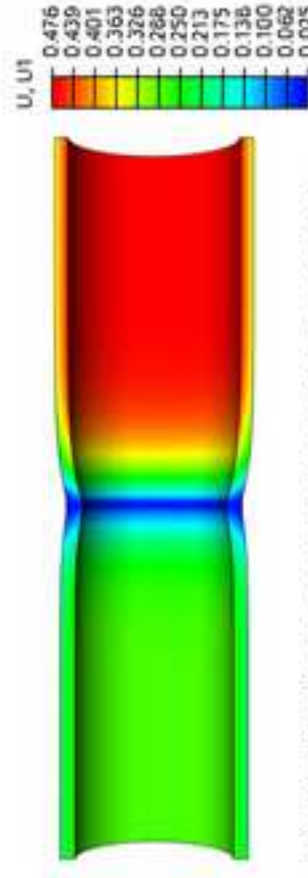
(d) Distal artery to prosthetic graft model



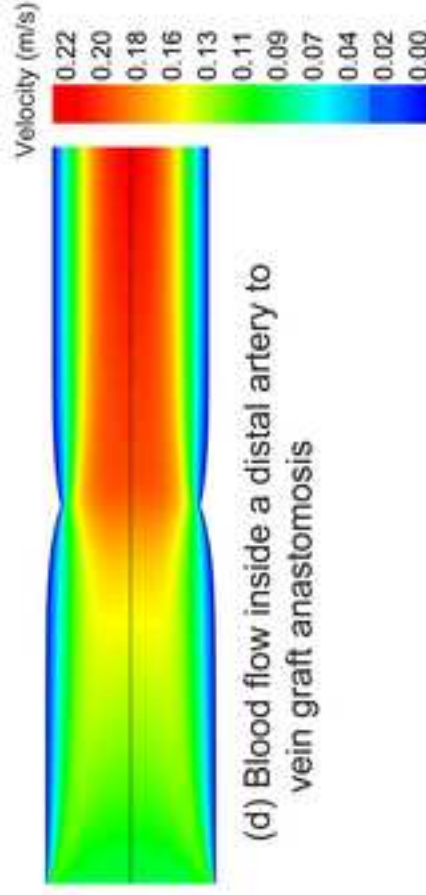
(a) Blood flow inside a proximal anastomosis of artery to vein graft



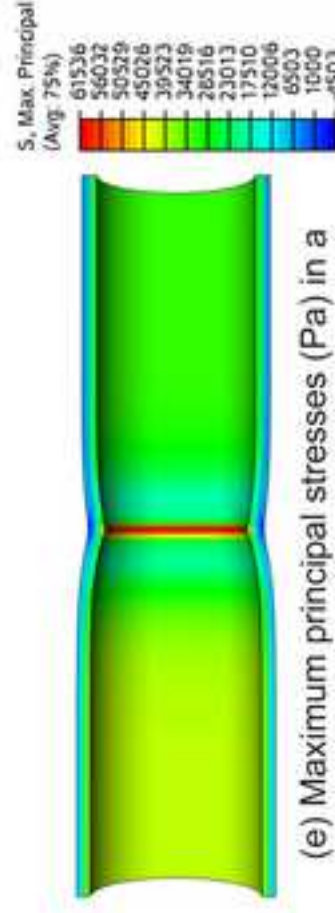
(b) Maximum principal stresses (Pa) in a proximal anastomosis of artery to vein graft



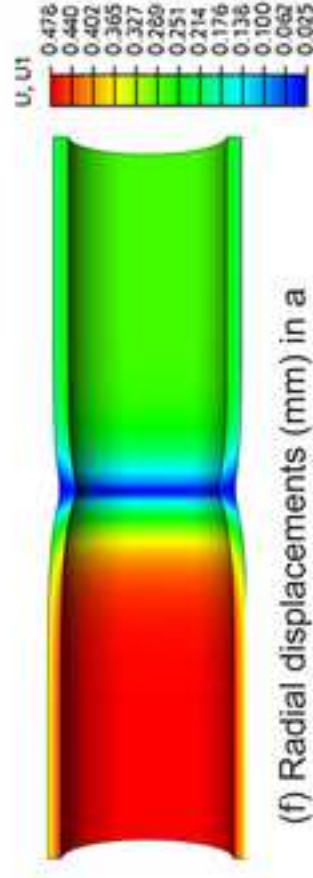
(c) Radial displacements (mm) in a proximal anastomosis of artery to vein graft



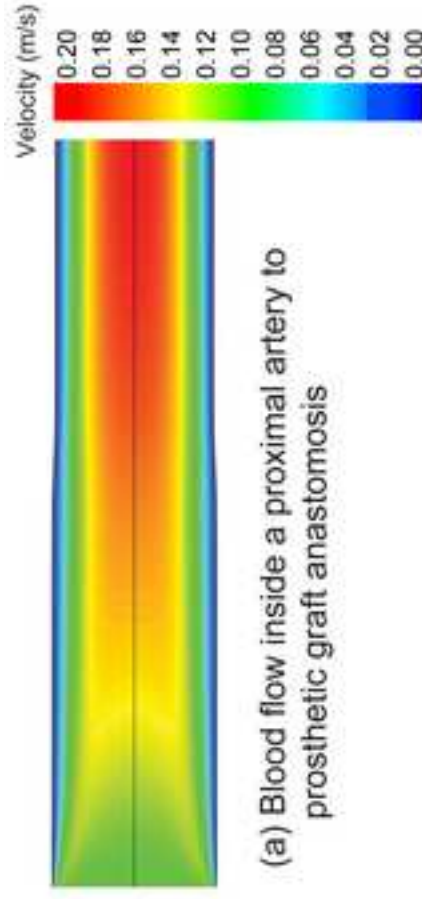
(d) Blood flow inside a distal artery to vein graft anastomosis



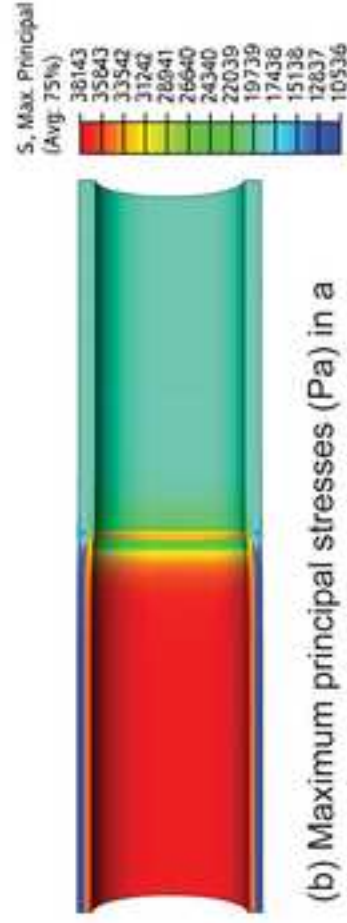
(e) Maximum principal stresses (Pa) in a distal artery to vein graft anastomosis



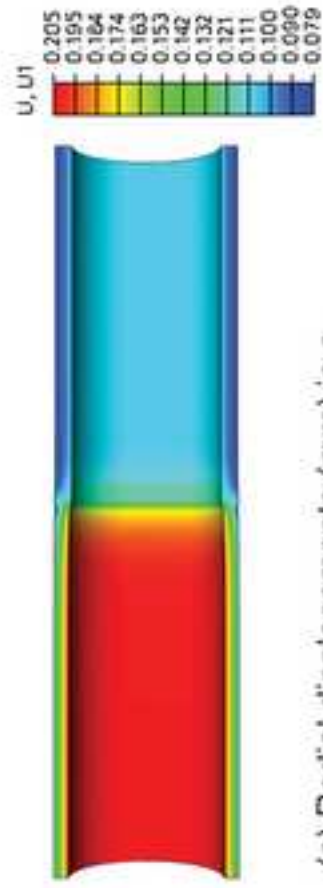
(f) Radial displacements (mm) in a distal artery to vein graft anastomosis



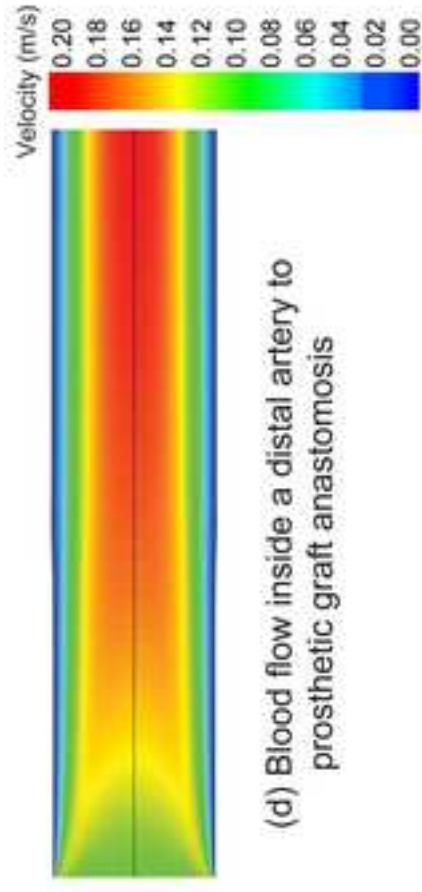
(a) Blood flow inside a proximal artery to prosthetic graft anastomosis



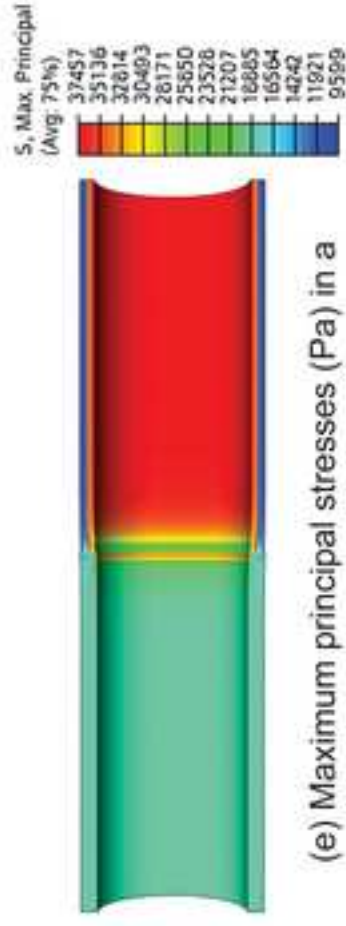
(b) Maximum principal stresses (Pa) in a proximal artery to prosthetic graft



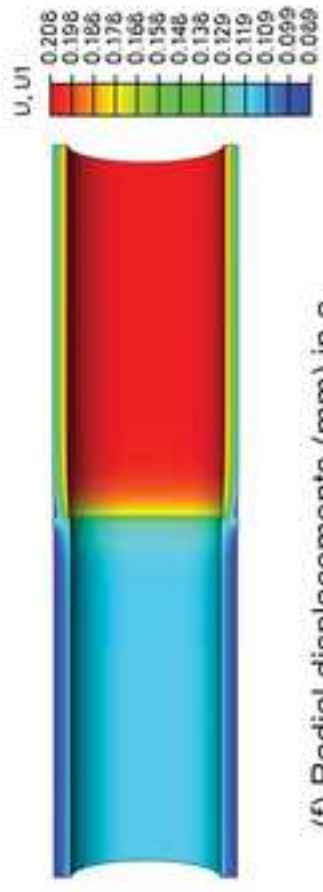
(c) Radial displacements (mm) in a proximal artery to prosthetic graft



(d) Blood flow inside a distal artery to prosthetic graft anastomosis



(e) Maximum principal stresses (Pa) in a distal artery to prosthetic graft



(f) Radial displacements (mm) in a distal artery to prosthetic graft